View metadata, citation and similar papers at core.ac.uk
brought to you by CORE
provided by Xiamen University Institutional Repository

Most stable structure of fullerene[20] and its novel activity toward addition of alkene: A theoretical study

Congjie Zhang[a] and Wenxiu Sun
School of Chemistry and Materials Science, Shaanxi Normal University, Xi'an 710062, China

Zexing Cao[b]
Department of Chemistry, State Key Laboratory for Physical Chemistry of Solid Surface, Xiamen University, Xiamen 361005, China

(Received 11 January 2007; accepted 21 February 2007; published online 11 April 2007)

Structures and stabilities of fullerene C_{20} and C_{20}^- have been investigated by the density functional theory and CCSD(T) calculations. In consideration of the Jahn-Teller distortion of I_h-symmetric C_{20}, possible subgroup symmetries have been used in the full geometry optimization. On the basis of relative energetics, vibrational analyses, and electron affinities, fullerenes C_{20} and C_{20}^- have most stable D_{2h} and C_i structures, respectively. The controversy on the relative stability of fullerene[20] arises from the use of different subgroups in calculation and the basis set dependence in vibrational analysis. Predicted nucleus-independent chemical shift values show that the most stable fullerene C_{20} and its derivatives $C_{20}(C_2H_2)_n$ and $C_{20}(C_2H_4)_n$ ($n=1-3$) exhibit remarkable aromaticity, while $C_{20}(C_2H_2)_4$ and $C_{20}(C_2H_4)_4$ have no spherical aromaticity. The C_{20} (D_{2h}) cage has remarkable activity toward the addition of olefin, and such feasibility of the addition reaction is ascribed to strong bonding interactions among frontier molecular orbitals from C_{20} and olefin. Calculations indicate that both $C_{20}(C_2H_2)_n$ and $C_{20}(C_2H_4)_n$ have similar features in electronic spectra. © *2007 American Institute of Physics*. [DOI: 10.1063/1.2716642]

I. INTRODUCTION

Since the discovery of C_{60} in 1985,[1] other fullerenes smaller than C_{60} have been attracting considerable interest both experimentally and theoretically.[2–8] Because smaller fullerenes with respect to C_{60} have strained pentagons, they are quite labile. Their synthesis and isolation in macroscopic quantities have been found to be extremely difficult experimentally.[9,10] In 2004, Xie *et al.* successfully prepared the first smaller fullerene derivative $C_{50}Cl_{10}$ in milligram quantities.[11] Spectroscopic characterization in combination with theoretical calculations show that the $C_{50}Cl_{10}$ cage is of D_{5h} symmetry and the C_{50} core comprises two C_{20} capes and five C_2 units around the equator.[12,13]

If a closed polyhedron requires that each vertex has a coordination index of 3 and the faces are pentagons and (or) hexagons, then according to Euler's theorem such a cage of 20-atom carbon cluster will comprise twelve pentagons and it is of I_h symmetry.

The C_{20} cluster, the smallest fullerene, has been extensively studied theoretically. Many *ab initio* and density functional theory (DFT) calculations have been directed toward the structure and the stability of its isomers: ring, bowl, and fullerene. However, the various theoretical calculations present inconsistent results.[14–19] Within the molecule orbital (MO) theory formalism, the I_h-symmetric C_{20} has the fourfold degenerate highest occupied MO (HOMO), while only two electrons are populated into these HOMOs. Presumably, such high symmetry will lower due to the Jahn-Teller effect.[20,21] In consideration of the Jahn-Teller distortion, certain low-symmetric isomers in D_{5d}, D_{3d}, D_{2h}, C_{2h}, C_2, and C_i subgroups of I_h have been investigated in previous calculations. Previous self-consistent field optimization located a structure with C_2 symmetry, while the local density approximation optimization yielded a structure with C_i symmetry.[14,15] A D_{3d}-symmetric structure optimized at the B3LYP/cc-PVDZ level was found to be unstable with two degenerate imaginary frequencies. At the same level of theory, two isomers with C_{2h} and C_i symmetry were predicted to be stable minima on the potential energy surface, and the C_i species are slightly lower in energy than the C_{2h} structure by 0.08 kcal mol^{-1}.[17]

In 2000, the smallest possible fullerene C_{20} was generated and characterized in the gas phase.[7] The hybrid-DFT calculations and theoretical analyses on the photoelectron spectra of C_{20}^- concluded that the cage structure with C_{2h} symmetry should be one of the species observed experimentally while the most stable structure predicted for C_{20}^- is of C_i symmetry.[22] At the restricted open shell Hartree-Fock level, the D_{3d}- and D_{2h}-symmetric isomers have relatively high stabilities.[23] The D_{3d} structure was further investigated by *ab initio* and DFT methods.[24,25] The adiabatic detachment energy (ADE) of C_{20}^- has been determined by the DFT calculation with the cc-pVTZ basis set,[24] and the predicted ADE is in agreement with the experimental values.[7] Recently, the B3LYP functional calculations based on a C_i-symmetric cage of C_{20} also predict the electron affinity in good agreement with the observed value.[26] The B3LYP/6-31G energetic analysis of C_{20} isomers indicates that the fullerene with D_{2h} symmetry has relatively high stability among cage isomers,

[a]Electronic mail: zcjwh@snnu.edu.cn
[b]Electronic mail: zxcao@xmu.edu.cn

 © 2007 American Institute of Physics

Downloaded 12 Jun 2011 to 219.229.31.19. Redistribution subject to AIP license or copyright; see http://jcp.aip.org/about/rights_and_permissions

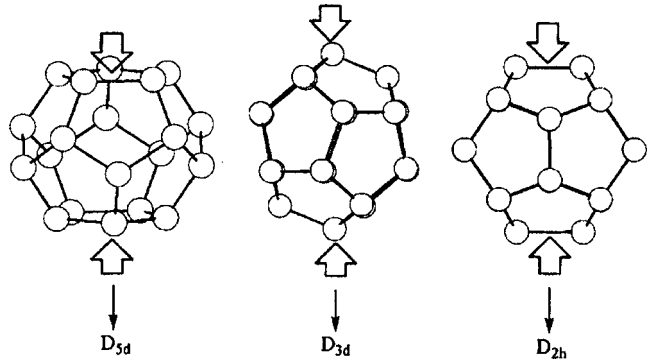

FIG. 1. The scheme of Jahn-Teller distortion of C_{20} with I_h symmetry.

but the D_{2h} structure has been predicted to have one imaginary frequency.[27] At B3LYP/6-31G* and MP2/6-31G* levels, five cage structures of C_{20} with C_2, C_i, C_{2h}, D_{2h}, and D_{3d} symmetries have been predicted to be true minima.[28] Such controversy on the relative stabilities of C_{20} cages also was presented in a recent review.[29]

In the present work, extensive *ab initio* and DFT calculations on fullerene isomers of C_{20} and their derivatives have been performed. Relative stabilities of possible isomers of fullerene[20]and the reaction activity of the most stable fullerene[20] toward the addition of olefin have been explored.

II. COMPUTATIONAL DETAILS

The smallest possible fullerene C_{20} consists of twelve solely pentagons and its highest possible symmetry is I_h. Such high symmetric isomer will undergo the Jahn-Teller distortion and decrease its symmetry. As Fig. 1 displays, when the distortion arises from compressing a couple of opposite faces, vertices, and bonds of fullerene C_{20}, the I_h symmetry will be reduced to D_{5d}, D_{3d}, and D_{2h}, respectively. In addition to the D_{5d}, D_{3d}, and D_{2h} structures, their lower subgroup symmetric structures such as C_{2h}, C_2, C_i, C_s, C_1, C_{5v}, C_{3v}, D_2, and C_{2v} have also been considered in the calculation. As a result, twelve isomers of fullerene C_{20} have been examined and the nature of optimized structures has been assessed by vibrational frequency analyses. The hybrid B3LYP functional in combination of 6-311+G**, 6-31G*, and cc-PVDZ basis sets has been used in full geometry optimization and frequency calculations. For lower-energy D_{3d}, D_{2h}, C_{2h}, C_2, and C_i isomers, the single point energy calculations at the CCSD(T)/cc-PVDZ level of theory have been performed based on the B3LYP/6-311+G**-optimized geometries.

In consideration of the Jahn-Teller distortion for the C_{20}^- structures with D_{5d}, D_{3d}, C_{5v}, and C_{3v} symmetries, only eight other structures of C_{20}^- have been investigated at the same theoretical level. The electron affinity (EA) of C_{20} has been calculated by B3LYP/6-311+G**, B3LYP/6-31G*, and B3LYP/aug-cc-PVTZ//B3LYP/6-311+G**.

The adducts of the most stable fullerene[20] with C_2H_2 and C_2H_4 have been studied by B3LYP/6-311+G**. For the most stable isomers of fullerene C_{20}, $C_{20}(C_2H_2)_n$, and $C_{20}(C_2H_4)_n$ $(n=1-4)$, their nucleus-independent chemical shift (NICS) and excited-state properties have been calculated by gauge-independent atomic orbital (GIAO) and time-dependent density functional theory (TD-DFT) approaches at the B3LYP/6-311+G** level of theory, respectively. All calculations are performed by GAUSSIAN 03 program.[30]

III. RESULTS AND DISCUSSION

A. Structures and stabilities of C_{20} and C_{20}^-

The symmetry, electronic state, the number of imaginary frequency, and total energies of twelve isomers of fullerene C_{20} and eight structures of C_{20}^- optimized by the B3LYP calculation with 6-311+G**, 6-31G*, and cc-PVDZ basis sets are collected in Table I. For comparison, the single point energies at the CCSD(T)/cc-PVDZ level at the B3LYP/6-311+G** optimized geometries are incorporated into Table I.

As can be seen from Table I, at the B3LYP/6-311+G** level, only D_{2h}, D_2, and C_{2v} isomers of C_{20} and C_i isomer of C_{20}^- are stable without imaginary frequency, while other structures are not stable due to existence of imaginary frequency. Notice that D_{2h}, D_2, and C_{2v} isomers of C_{20} are isoenergetic and they have almost the same geometrical parameters. Therefore, such three isomers, arising from use of different subgroups in calculation, should belong to the same structure. In addition, B3LYP/6-31G* calculations predict that C_{2h} and C_2 isomers of C_{20} are minima on the potential energy surface, and they are almost isoenergetic with respect to the D_{2h} isomer. The maximal difference of the corresponding bond distances between D_{2h} and C_{2h} isomers is less than 0.0003 Å. Further geometry optimizations and vibrational analyses for five low-energy isomers D_{3d}, D_{2h}, C_{2h}, C_2, and C_i by B3LYP/cc-PVDZ indicate that D_{2h} and C_2 isomers are stable structures. Both isoenergetic species have almost the same geometries and they should belong to the same structure. At the CCSD(T)/cc-PVDZ level of theory, D_{2h}, C_{2h}, and C_2 isomers are also isoenergetic. Present calculations show that the ground state of fullerene[20] should be of D_{2h} symmetry. Negligible discrepancies in energy and in geometry among the lower-energy isomers can be ascribed to the use of distinct subgroups in the calculation.

The most stable structure of C_{20}^- is of C_i symmetry at both B3LYP/6-311+G** and B3LYP/6-31G* levels, which agrees with the previous theoretical results.[22,25] The AEA of C_{20} determined by B3LYP/6-311+G** and B3LYP/aug-cc-PVTZ‖B3LYP/6-311+G** calculations are 2.43 and 2.35 eV, respectively, which are in good agreement with the previous theoretical values (2.36 and 2.30 eV) (Ref. 25) and the experiment value (2.25 eV).[7] As Table I displays, the predicted adiabatic electron affinity by B3LYP/6-31G* is 1.78 eV, quite lower than the observed value, which suggests that the diffuse functions are important for the calculation of the anionic species.

Figure 2 displays the ground-state geometries of fullerene[20] and its anion. Although vibrational analyses depend on methodology and use of basis set, all calculations conclude that the ground states of the C_{20} fullerene and its anion should have D_{2h} and C_i structures, respectively. In the D_{2h} and C_i isomers, the C–C bond length varies from

Downloaded 12 Jun 2011 to 219.229.31.19. Redistribution subject to AIP license or copyright; see http://jcp.aip.org/about/rights_and_permissions

TABLE I. Symmetries, electronic states, and total energies (in a.u) of C_{20} and C_{20}^- and adiabatic electron affinites (AEAs in eV) of C_{20}.

Isomers	State	B3LYP[a] 6-311+G**	B3LYP[a] 6-31G*	cc-PVDZ	CCSD(T)	AEA
C_{20} (D_{5d})	$^3A_{1g}$	−761.595 82(4)	−761.437 72(4)			
C_{20} (C_{5v})	$^3A_1$	−761.595 52(4)	−761.473 72(4)			
C_{20} (D_{3d})	$^1A_{1g}$	−761.597 88(2)	−761.440 93(2)	−761.498 68(2)	−759.400 92	
C_{20} (C_{3v})	$^1A_1$	−761.597 88(2)	−761.440 93(2)			
C_{20} (D_{2h})	^1A_g	−761.602 35(0)	−761.444 44(0)	−761.502 53(0)	−759.410 35	2.43[b] 1.78[c] 2.35[d] 2.25[e]
C_{20} (D_2)	^1A	−761.602 35(0)	−761.444 44(0)			
C_{20} (C_{2h})	^1A_g	−761.602 07(1)	−761.444 20(0)	−761.502 28(1)	−759.410 45	
C_{20} (C_{2v})	$^1A_1$	−761.602 35(0)	−761.444 44(0)			
C_{20} (C_2)	^1A	−761.602 02(1)	−761.444 16(0)	−761.502 53(0)	−759.410 45	
C_{20} (C_i)	^1A_g	−761.602 27(1)	−761.444 81(1)	−761.502 44(1)	−759.410 06	
C_{20} (C_s)	$^1A'$	−761.597 75(2)	−761.440 81(2)			
C_{20} (C_1)	^1A	−761.602 21(1)	−761.444 80(1)			
C_{20}^- (D_{2h})	^2A_u	−761.686 86(2)	−761.503 77(2)			
C_{20}^- (D_2)	$^2B_1$	−761.684 36(2)				
C_{20}^- (C_{2h})	^2A_u	−761.686 70(2)	−761.503 63(2)			
C_{20}^- (C_{2v})	$^2A_2$	−761.686 86(2)	−761.503 77(2)			
C_{20}^- (C_2)	^2A	−761.686 86(2)				
C_{20}^- (C_i)	^2A_u	−761.687 94(0)	−761.506 75(0)			
C_{20}^- (C_s)	$^2A'$	−761.686 25(2)				
C_{20}^- (C_1)	^2A	−761.686 84(2)				

[a]The number of imaginary frequency modes in parentheses.
[b]B3LYP/6-311+G**.
[c]B3LYP/6-31G*.
[d]B3LYP/aug-cc-PVTZ//B3LYP/6-311+G**.
[e]Experimental value.

1.397 to 1.535 Å, and no notable geometrical change occurs as the neutral C_{20} accommodates one electron.

According to the group representation theory in chemistry, we can easily deduce that there are 54 kinds of vibrational modes for C_{20} with D_{2h} symmetry, which are $9a_g+6b_{1g}+6b_{2g}+6b_{3g}+6a_u+7b_{1u}+7b_{2u}+7b_{3u}$. Among these normal modes, only 21 b_{1u}, b_{2u}, and b_{3u} vibrational modes are IR active. The lowest frequency and other nine strong vibrational frequencies for $C_{20}(D_{2h})$ and $C_{20}^-(C_i)$ are listed in Table II. Between 600 and 800 cm^{-1}, there are 12 vibrational bands at $600(b_{1g})$, $625(a_u)$, $650(b_{2u})$, $651(a_u)$, $667(b_{2u})$, $721(a_g)$, $723(b_{3g})$, $733(b_{1u})$, $734(b_{2g})$, $741(b_{3u})$, $782(b_{1g})$, and $788(b_{3g})$. The predicted 721 cm^{-1} (a_g) band from the symmetrical bond bending is in agreement with previous theoretical value of 643 cm^{-1} (a_g) (Ref. 19) and the spacing of 730 ± 70 cm^{-1} for the Franck-Condon progression observed experimentally.[7] Both C_{20} and C_{20}^- exhibit similar IR spectroscopic features as shown in Table II.

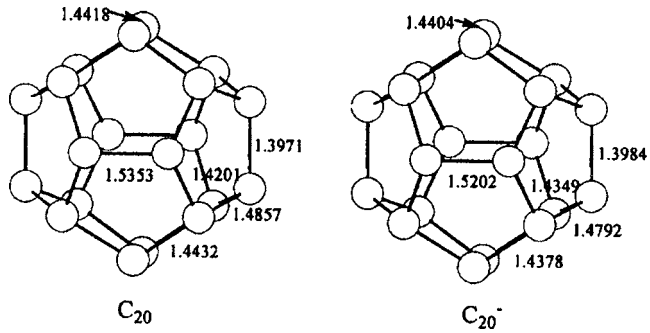

FIG. 2. B3LYP-optimized geometries of the most stable fullerenes C_{20} (D_{2h}) and $C_{20}^-(C_i)$.

B. Structures and stabilities of adducts $C_{20}(C_2H_2)_n$ and $C_{20}(C_2H_4)_n$ (n=1−4)

As discussed above, the most stable cage of C_{20} is of D_{2h} symmetry. In order to have insight to its reactivity, we examine the relevant frontier MOs of the D_{2h} structure. Six frontier MOs are depicted in Fig. 3. Figure 4 displays the orbital correlation scheme for interactions among frontier MOs of C_{20} (D_{2h}) with C_2H_2 and C_2H_4. As Figs. 3 and 4 display, the local phase patterns of occupied 57th, 59th, and 60th MOs of C_{20} match those of the lowest unoccupied MOs (LUMOs) of ethyne and ethene, and these frontier MOs are close in energy. Presumably, there are strong bonding interactions of C_{20} (D_{2h}) with C_2H_2 and C_2H_4. Similarly, strong bonding interactions may arise from the unoccupied frontier MOs of C_{20} and HOMOs of C_2H_2 and C_2H_4, which will enhance intermolecular bonding and facilitate the formation of adducts $C_{20}(C_2H_2)_n$ and $C_{20}(C_2H_4)_n$. In general, only four C_2

Downloaded 12 Jun 2011 to 219.229.31.19. Redistribution subject to AIP license or copyright; see http://jcp.aip.org/about/rights_and_permissions

TABLE II. Selected vibrational frequencies (in cm^{-1}) and IR intensities ($km\,mol^{-1}$) of C_{20} (D_{2h}), C_{20}^{-} (C_i), $C_{20}(C_2H_2)_n$, and $C_{20}(C_2H_4)_n$ ($n=1-4$).

C_{20} (D_{2h})	C_{20}^{-} (C_i)	$C_{20}(C_2H_2)$	$C_{20}(C_2H_2)_2$	$C_{20}(C_2H_2)_3$
$32(b_{3g},0)$	$179(a_g,0)$	$245(b_1,2)$	$207(b_{1u},7)$	$200(b_3,7)$
$733(b_{1u},15)$	$736(a_u,90)$	$695(b_2,13)$	$521(b_{3u},89)$	$508(b_2,98)$
$741(b_{3u},55)$	$884(a_u,39)$	$725(a_1,107)$	$529(b_{1u},41)$	$606(b_1,60)$
$898(b_{1u},17)$	$890(a_u,30)$	$817(b_2,20)$	$708(b_{3u},175)$	$734(b_2,193)$
$909(b_{2u},26)$	$909(a_u,30)$	$928(b_1,40)$	$786(b_{2u},49)$	$861(b_2,66)$
$1224(b_{3u},60)$	$1164(a_u,33)$	$1313(a_1,15)$	$929(b_{1u},65)$	$863(b_1,66)$
$1233(b_{2u},21)$	$1215(a_u,87)$	$1273(a_1,63)$	$1280(b_{3u},128)$	$1213(b_2,47)$
$1289(b_{3u},13)$	$1222(a_u,22)$	$1333(b_1,89)$	$1312(b_{3u},57)$	$1271(b_2,100)$
$1352(b_{3u},68)$	$1297(a_u,91)$	$1377(b_1,21)$	$1319(b_{1u},33)$	$1297(b_2,74)$
$1356(b_{2u},140)$	$1348(a_u,102)$	$3213(a_1,27)$	$3205(b_{3u},78)$	$3202(b_2,92)$
$C_{20}(C_2H_2)_4$	$C_{20}(C_2H_4)$	$C_{20}(C_2H_4)_2$	$C_{20}(C_2H_4)_3$	$C_{20}(C_2H_4)_4$
$197(b_{1u},2)$	$181(a_1,0)$	$168(a_u,0)$	$75(a_2,0)$	$169(a_u,0)$
$487(b_{2u},99)$	$726(a_1,98)$	$517(b_{3u},79)$	$472(b_2,55)$	$491(b_{2u},71)$
$699(b_{2u},75)$	$741(a_1,33)$	$520(b_{1u},47)$	$504(b_2,58)$	$669(b_{3u},61)$
$723(b_{2u},203)$	$878(a_1,17)$	$705(b_{3u},207)$	$669(b_2,68)$	$711(b_{2u},315)$
$818(b_{2u},136)$	$899(b_1,28)$	$891(b_{3u},41)$	$708(b_2,93)$	$773(b_{2u},111)$
$849(b_{1u},81)$	$1272(a_1,51)$	$903(b_{1u},38)$	$1144(b_2,68)$	$838(b_{3u},83)$
$1370(b_{3u},117)$	$1335(b_1,94)$	$1279(b_{3u},128)$	$1230(b_2,73)$	$1373(b_{3u},138)$
$1604(b_{2u},63)$	$1375(b_1,18)$	$1325(b_{1u},34)$	$3055(a_1,47)$	$3047(b_{1u},61)$
$3192(b_{3u},119)$	$3065(b_2,23)$	$3062(b_{2u},49)$	$3060(b_2,144)$	$3052(b_{3u},181)$
$3218(b_{2u},68)$	$3096(a_1,55)$	$3066(b_{3u},134)$	$3067(a_1,54)$	$3074(b_{2u},175)$

units in C_{20} can serve as active sites for olefin addition, and thus the number of ethyne and ethene in the adduct should not be greater than 4.

B3LYP/6-311+G**-optimized geometries of $C_{20}(C_2H_2)_n$ and $C_{20}(C_2H_4)_n$ ($n=1-4$) are shown in Fig. 5. Selected ten vibrational frequencies (corresponding to the lowest one and other strong IR bands) are incorporated into Table II. Predicted reaction energies and NICS values are given in Table III.

As Fig. 5 shows, CC bonds of subunits C_2H_2 and C_2H_4 in the adducts $C_{20}(C_2H_2)_n$ and $C_{20}(C_2H_4)_n$ ($n=1-4$) have typical characters of a double bond and a single bond, respectively. The C–C separation of C_2 unit bonding olefin in the C_{20} core increases remarkably with respect to fullerene[20]. For example, such C–C bond distances in $C_{20}(C_2H_2)_n$ ($n=1-4$) are 1.609, 1.642, 1.656 (1.693), and 1.610 (1.673) Å, respectively, as the number of ethyne increases from $n=1$ to $n=4$. They are longer than that of 1.397 Å in C_{20} (Fig. 2). The adducts $C_{20}(C_2H_4)_n$ ($n=1-4$) have similar geometrical features with $C_{20}(C_2H_2)_n$ ($n=1-4$). Frequency calculations in Table II show that these optimized structures of $C_{20}(C_2H_2)_n$ and $C_{20}(C_2H_4)_n$ ($n=1-4$) in Fig. 5 are stable species without vibrational imaginary frequency.

In order to explore the stability of such adducts, we calculated the energy gap between HOMO and LUMO and reaction energies for the addition Reactions (1) and (2) as follows:

$$C_{20} + nC_2H_2 \rightarrow C_{20}(C_2H_2)_n \quad (n = 1-4), \tag{1}$$

$$C_{20} + nC_2H_4 \rightarrow C_{20}(C_2H_4)_n \quad (n = 1-4). \tag{2}$$

The reaction energies are defined as

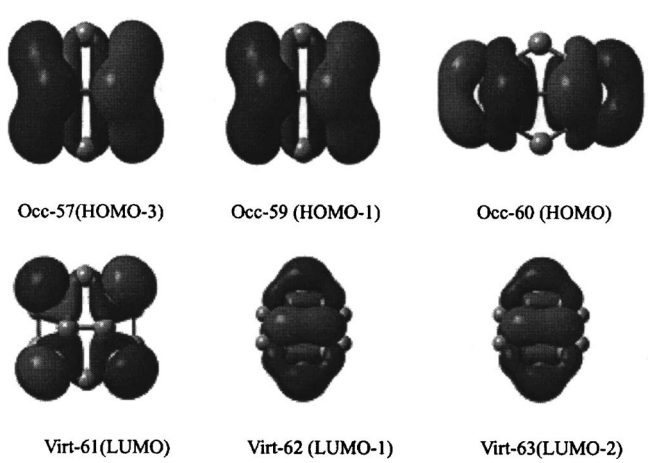

FIG. 3. Phase patterns of six frontier MOs of C_{20} (D_{2h}).

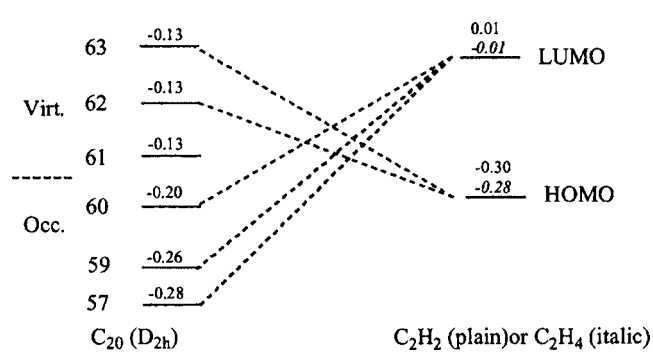

FIG. 4. The correlation scheme of frontier MOs between C_{20} and olefin.

Downloaded 12 Jun 2011 to 219.229.31.19. Redistribution subject to AIP license or copyright; see http://jcp.aip.org/about/rights_and_permissions

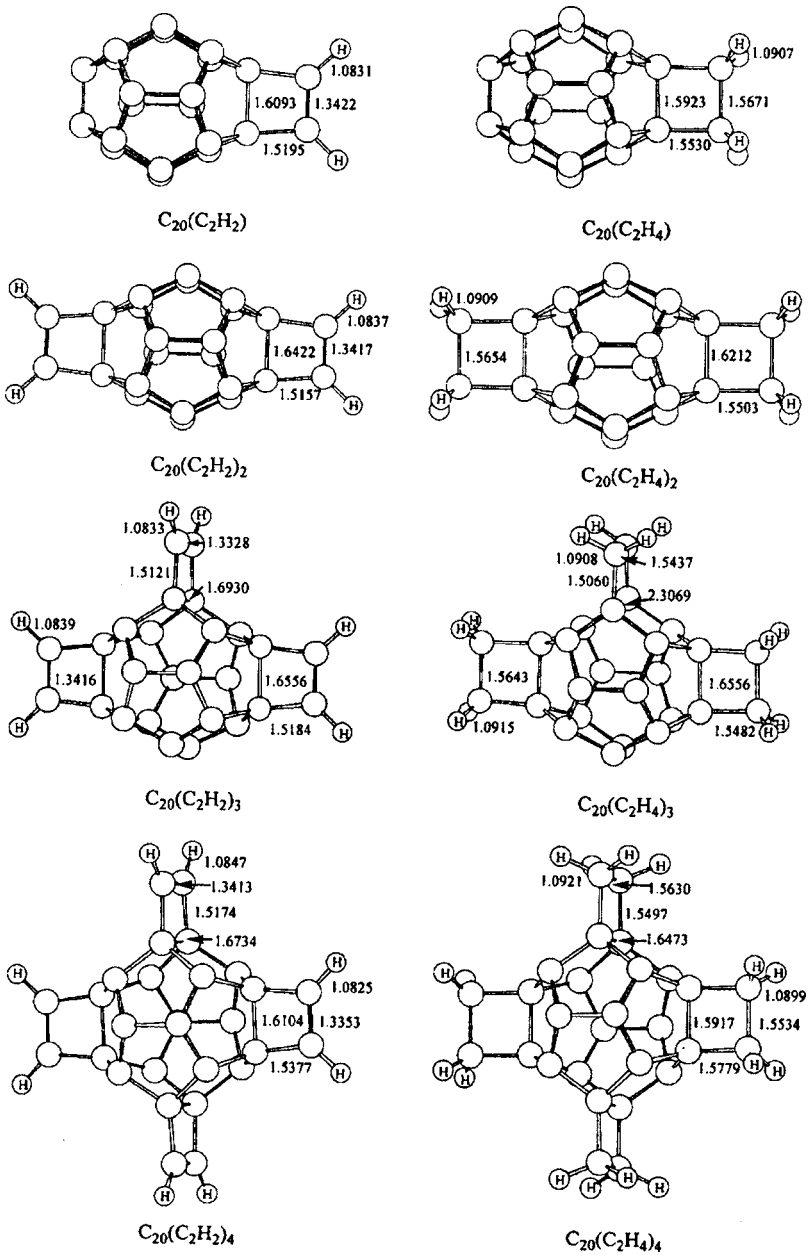

FIG. 5. B3LYP-optimized geometries of stable $C_{20}(C_2H_2)_n$ and $C_{20}(C_2H_4)_n$ ($n=1-4$).

$$\Delta H = [H(C_{20}(L)_n) - H(C_{20}) - nH(L)]/n, \quad (3)$$

where $L=C_2H_2$ and C_2H_4. The energy gaps and reaction energies are presented in Table III. As Table III indicates, the reaction energies are all negative for both $C_{20}(C_2H_2)_n$ and $C_{20}(C_2H_4)_n$, showing that such adducts have relatively high stability. As Fig. 4 shows, the strong bonding interactions among frontier MOs from C_{20} and olefin make such addition reaction facile in their ground states. The HOMO-LUMO

TABLE III. Reaction energies (ΔH in kcal mol^{-1}), energy gaps (in eV), and NICS values (in ppm) of $C_{20}(D_{2h})$, $C_{20}(C_2H_2)_n$, and $C_{20}(C_2H_4)_n$ ($n=1-4$).

Isomers	Symmetry	State	ΔH	HOMO	LUMO	Gap	NICS
C_{20}	D_{2h}	^1A_g		−0.203	−0.133	1.90	−24.0
$C_{20}(C_2H_2)$	C_{2v}	$^1A_1$	−64.55	−0.213	−0.124	2.42	−38.9
$C_{20}(C_2H_2)_2$	D_{2h}	^1A_g	−60.24	−0.213	−0.118	2.58	−39.7
$C_{20}(C_2H_2)_3$	C_{2v}	$^1A_1$	−48.60	−0.202	−0.118	2.29	−20.9
$C_{20}(C_2H_2)_4$	D_{2h}	^1A_g	−36.63	−0.189	−0.149	1.09	33.3
$C_{20}(C_2H_4)$	C_{2v}	$^1A_1$	−55.95	−0.211	−0.121	2.45	−39.6
$C_{20}(C_2H_4)_2$	D_{2h}	^1A_g	−51.04	−0.207	−0.113	2.56	−40.9
$C_{20}(C_2H_4)_3$	C_{2v}	$^1A_1$	−37.69	−0.188	−0.101	2.37	−32.8
$C_{20}(C_2H_4)_4$	D_{2h}	^1A_g	−27.66	−0.180	−0.142	1.03	51.1

Downloaded 12 Jun 2011 to 219.229.31.19. Redistribution subject to AIP license or copyright; see http://jcp.aip.org/about/rights_and_permissions

TABLE IV. Vertical transition energies (λ in nm) and oscillator strengths (f) of $C_{20}(D_{2h})$, $C_{20}(C_2H_2)_n$, and $C_{20}(C_2H_4)_n$.

Species	λ	f	Transition	Species	λ	f	Transition
$C_{20}(D_{2h})$	436.5	0.0032	$X\,^1A_g \rightarrow A\,^1B_{2u}$	$C_{20}(C_2H_4)$	637.0	0.0041	$X\,^1A_1 \rightarrow A\,^1B_2$
	430.7	0.0183	$X\,^1A_g \rightarrow B\,^1B_{3u}$		472.6	0.0138	$X\,^1A_1 \rightarrow B\,^1B_1$
$C_{20}(C_2H_2)$	639.8	0.0035	$X\,^1A_1 \rightarrow A\,^1B_2$		452.6	0.0097	$X\,^1A_1 \rightarrow C\,^1A_1$
	473.0	0.0144	$X\,^1A_1 \rightarrow B\,^1B_1$	$C_{20}(C_2H_4)_2$	584.5	0.0280	$X\,^1A_g \rightarrow A\,^1B_{1u}$
	450.8	0.0082	$X\,^1A_1 \rightarrow C\,^1A_1$		532.1	0.0166	$X\,^1A_g \rightarrow B\,^1B_{3u}$
$C_{20}(C_2H_2)_2$	578.2	0.0289	$X\,^1A_g \rightarrow A\,^1B_{1u}$	$C_{20}(C_2H_4)_3$	749.4	0.0226	$X\,^1A_1 \rightarrow A\,^1B_2$
	521.5	0.0128	$X\,^1A_g \rightarrow B\,^1B_{3u}$		651.7	0.0197	$X\,^1A_1 \rightarrow B\,^1B_1$
$C_{20}(C_2H_2)_3$	799.0	0.0140	$X\,^1A_1 \rightarrow A\,^1B_2$		485.3	0.0082	$X\,^1A_1 \rightarrow C\,^1A_1$
	638.3	0.0115	$X\,^1A_1 \rightarrow B\,^1B_1$		435.0	0.0007	$X\,^1A_1 \rightarrow D\,^1B_2$
	520.6	0.0542	$X\,^1A_1 \rightarrow C\,^1B_1$		424.2	0.0005	$X\,^1A_1 \rightarrow B\,^1B_1$
	448.7	0.0868	$X\,^1A_1 \rightarrow D\,^1B_2$		401.5	0.0234	$X\,^1A_1 \rightarrow C\,^1B_1$
$C_{20}(C_2H_2)_4$	2748.4	0.0036	$X\,^1A_g \rightarrow A\,^1B_{2u}$	$C_{20}(C_2H_4)_4$	2033.7	0.0061	$X\,^1A_g \rightarrow A\,^1B_{2u}$
	847.7	0.0031	$X\,^1A_g \rightarrow B\,^1B_{3u}$		766.8	0.0033	$X\,^1A_g \rightarrow B\,^1B_{3u}$
	599.1	0.0477	$X\,^1A_g \rightarrow C\,^1B_{2u}$		577.4	0.0434	$X\,^1A_g \rightarrow C\,^1B_{2u}$
	482.4	0.0084	$X\,^1A_g \rightarrow D\,^1B_{3u}$		482.0	0.0109	$X\,^1A_g \rightarrow D\,^1B_{3u}$
	454.3	0.0011	$X\,^1A_g \rightarrow B\,^1B_{3u}$		419.6	0.0605	$X\,^1A_g \rightarrow E\,^1B_{3u}$
	419.6	0.0137	$X\,^1A_g \rightarrow F\,^1B_{3u}$				

gaps for $C_{20}(C_2H_2)_n$ and $C_{20}(C_2H_4)_n$ ($n=1-3$) are larger than that of C_{20}, while the adducts $C_{20}(C_2H_2)_4$ and $C_{20}(C_2H_4)_4$ have the smallest HOMO-LUMO splitting due to strong strained interactions.

C. Aromaticity of $C_{20}(D_{2h})$, $C_{20}(C_2H_2)_n$, and $C_{20}(C_2H_4)_n$ ($n=1-4$)

According to the Hirsch's $2(N+1)^2$ electron counting rule for spherical molecules,[31] the C_{20}^{2+} should be an aromatic fullerene. Similarly, the adducts $C_{20}(C_2H_2)$ and $C_{20}(C_2H_4)$ are also of the same aromaticity. In previous studies,[32] the NICS values have been extensively used for description of aromaticity. The NICS values at the center of C_{20} core for C_{20} and its derivatives $C_{20}(C_2H_2)_n$ and $C_{20}(C_2H_4)_n$ ($n=1-4$) have been calculated by GIAO B3LYP/6-311+G**, and predicted NICS values are incorporated into Table III. As Table III displays, the calculated NICS values for C_{20}, $C_{20}(C_2H_2)_n$ and $C_{20}(C_2H_4)_n$ ($n=1-3$) range from −20.9 to −40.9 ppm, showing that they are aromatic species. For $C_{20}(C_2H_2)_4$ and $C_{20}(C_2H_4)_4$, both species have positive NICS values of 33.3 and 51.1 ppm, respectively, and they have no spherical aromaticity. As Table III shows, the adducts $C_{20}(C_2H_2)_n$ and $C_{20}(C_2H_4)_n$ ($n=1$ and 2) generally have more negative NICS values than other species, and thus they should have relatively high aromaticity. Actually, in these adducts there are 18 or 16 electrons for delocalized π bonding, and this is consistent with the $2(N+1)^2$ or 8 electron counting rule for spherical molecules.[31–33]

D. Electronic spectra of $C_{20}(D_{2h})$, $C_{20}(C_2H_2)_n$, and $C_{20}(C_2H_4)_n$ ($n=1-4$)

The vertical transition energies of $C_{20}(D_{2h})$, $C_{20}(C_2H_2)_n$, and $C_{20}(C_2H_4)_n$ ($n=1-4$) are calculated by the TD-B3LYP approach with the 6-311+G** basis set, and the bands with wave lengths larger than 400 nm are summarized in Table IV. As can be seen from Table IV, for $C_{20}(D_{2h})$, strong absorptions at 436.5 and 430 nm arise from $X\,^1A_g \rightarrow A\,^1B_{2u}$ and $X\,^1A_g \rightarrow A\,^1B_{2u}$ transitions, respectively. The electronic spectra of $C_{20}(C_2H_2)_n$ and $C_{20}(C_2H_4)_n$ are quite similar. For instance, strong $X\,^1A_g \rightarrow A\,^1B_{1u}$ and $X\,^1A_g \rightarrow B\,^1B_{3u}$ transitions in the adducts appear at 578.2 and 521.5 nm for $C_{20}(C_2H_2)_2$ and at 584.5 and 532.1 nm for $C_{20}(C_2H_4)_2$, respectively.

IV. CONCLUSIONS

The structures and stabilities of fullerenes C_{20} and C_{20}^- have been systemically studied by DFT and sophisticated *ab initio* calculations. On the basis of relative energies, vibrational analyses, and electron affinities, the ground states of fullerenes C_{20} and C_{20}^- have been predicted to have D_{2h} and C_i structures, respectively. Electronic spectra and aromaticities of the most stable fullerene C_{20} and its derivatives of $C_{20}(C_2H_2)_n$ and $C_{20}(C_2H_4)_n$ ($n=1-4$) have been explored. Present calculations show that the fullerene C_{20} (D_{2h}) has high activity toward addition of olefin and the adducts $C_{20}(C_2H_2)_n$ and $C_{20}(C_2H_4)_n$ ($n=1-4$) have relatively high stabilities. Predicted NICS values indicate that C_{20}, $C_{20}(C_2H_2)_n$, and $C_{20}(C_2H_4)_n$ ($n=1-3$) are of aromaticity, while $C_{20}(C_2H_2)_4$ and $C_{20}(C_2H_4)_4$ have no spherical aromaticity. Both $C_{20}(C_2H_2)_n$ and $C_{20}(C_2H_4)_n$ ($n=1-4$) exhibit similar features in electronic spectra.

ACKNOWLEDGMENTS

This work was financially supported from State Key Laboratory for Physical Chemistry of Solid Surfaces (Xiamen University) (200504), the start-up fund of Shaanxi Normal University, the National Natural Science Foundation (Nos. 20673087, 20473062, and 20021002), and the Ministry of Science and Technology (2004CB719902).

[1] H. W. Kroto, J. R. Helth, S. C. O'Brien, R. F. Curl, and R. E. Samlley, Nature (London) **318**, 162 (1985).
[2] W. Weltner, Jr. and R. J. Van Zee, Chem. Rev. (Washington, D.C.) **89**, 1713 (1989).
[3] M. Feyereisen, M. Gutowski, and J. Simons, J. Chem. Phys. **96**, 2926 (1992).

Downloaded 12 Jun 2011 to 219.229.31.19. Redistribution subject to AIP license or copyright; see http://jcp.aip.org/about/rights_and_permissions

[4] N. Kurita, K. Kobayashi, H. Kumahora, K. Tago, and K. Ozawa, Chem. Phys. Lett. **188**, 181 (1992).
[5] J. R. Heath, Nature (London) **393**, 730 (1998).
[6] C. Piskoti, J. Yarger, and A. Zettl, Nature (London) **393**, 771 (1998).
[7] H. Prinzbach, A. Weiler, P. Landenberger, F. Wahl, J. Worth, L. T. Scott, M. D. Gelmont, D. Olevano, and B. V. Issendorff, Nature (London) **407**, 60 (2000).
[8] A. Van Orden and R. J. Saykally, Chem. Rev. (Washington, D.C.) **98**, 2313 (1998).
[9] Z. Wang, X. Ke, F. Zhu, M. Ruan, H. Chen, R. Huang, and L. Zheng, Phys. Lett. A **280**, 351 (2001).
[10] A. Koshio, M. Inakuma, T. Sugai, and H. Shinohara, J. Am. Chem. Soc. **122**, 398 (2000).
[11] S. Y. Xie, F. Gao, X. Lu, R. B. Huang, C. R. Wang, X. Zhang, M. L. Liu, S. L. Deng, and L. S. Zheng, Science **304**, 699 (2004).
[12] X. Lu, Z. Chen, W. Thiel, and P. V. R. Schleyer, J. Am. Chem. Soc. **126**, 14871 (2004).
[13] Z. Chen, Angew. Chem., Int. Ed. **43**, 4690 (2004).
[14] J. C. Grossman, L. Mitas, and K. Raghavachari, Phys. Rev. Lett. **75**, 3870 (1995).
[15] P. R. Taylor, E. Bylaska, J. H. Weare, and R. Kawai, Chem. Phys. Lett. **235**, 558 (1995).
[16] Z. Wang, P. Day, and R. Pachter, Chem. Phys. Lett. **248**, 121 (1996).
[17] M. L. Martin Jan, J. El-Yazal, and J. Francois, Chem. Phys. Lett. **248**, 345 (1996).
[18] E. J. Bylaska, P. R. Taylor, R. Kawai, and J. H. Weare, J. Phys. Chem. A **100**, 6966 (1996).
[19] S. Sokolova, A. Luchow, and J. B. Anderson, Chem. Phys. Lett. **323**, 229 (2000).
[20] B. N. Cyvin, E. Brendsdal, J. Brunvoll, and S. J. Cyvin, J. Mol. Struct. **352/353**, 481 (1995).
[21] G. Duskesas and S. Larsson, Theor. Chem. Acc. **97**, 110 (1997).
[22] M. Saito and Y. Miyamoto, Phys. Rev. Lett. **87**, 035503-1 (2001).
[23] B. Paulus, Phys. Chem. Chem. Phys. **5**, 3364 (2003).
[24] W. An, Y. Gao, S. Bulusu, and X. C. Zeng, J. Chem. Phys. **122**, 204109 (2005).
[25] G. Galli, F. Gygi, and J. C. Golaz, Phys. Rev. B **57**, 1860 (1998).
[26] J. Lu, S. Re, Y. Choe, S. Nagase, Y. Zhou, R. Han, L. Peng, X. Zhang, and X. Zhao, Phys. Rev. B **67**, 125415 (2003).
[27] C. Allison and K. A. Beran, J. Mol. Struct.: THEOCHEM **680**, 59 (2004).
[28] Z. Chen, T. Heine, H. Jiao, A. Hirsch, W. Thiel, and P. V. R. Schleyer, Chem.-Eur. J. **10**, 963 (2004).
[29] X. Lu and Z. Chen, Chem. Rev. (Washington, D.C.) **105**, 3643 (2005).
[30] M. J. Frisch, G. A. Trucks, H. B. Schlegel *et al.*, GAUSSIAN 03, Revision C.02 (Gaussian, Inc., Wallingford, CT, 2004).
[31] A. Hirsch, Z. Chen, and H. Jiao, Angew. Chem., Int. Ed. **39**, 3915 (2000).
[32] P. V. R. Schleyer, C. Maerker, A. Dransfeld, H. Jiao, and N. J. R. V. E. Hommes, J. Am. Chem. Soc. **118**, 6317 (1996).
[33] Z. Chen, H. Jiao, A. Hirsch, and P. V. R. Schleyer, Angew. Chem., Int. Ed. **41**, 4309 (2002).

Downloaded 12 Jun 2011 to 219.229.31.19. Redistribution subject to AIP license or copyright; see http://jcp.aip.org/about/rights_and_permissions